Precisely Controllable Artificial Muscle with Continuous Morphing based on "Breathing" of Supramolecular Columns

Zifan Yang, Jiahua Li, Xu Chen, Yining Fan, Jin Huang, Haifeng Yu, Shuang Yang,* and Er-Qiang Chen*

Skeletal muscles are natural motors executing sophisticated work through precise control of linear contraction. Although various liquid crystal polymers based artificial muscles have been designed, the mechanism based on mainly the order–disorder transition usually leads to discrete shape morphing, leaving arbitrary and precise deformation a huge challenge. Here, one novel photoresponsive hemiphasmidic side-chain liquid crystal polymer with a unique "breathing" columnar phase that enables continuous morphing is presented. Due to confinement inside the supramolecular columnar assembly, the cooperative movements of side-chains and backbones generate a significant negative thermal expansion and lead to temperature-controllable muscle-like elongation/contraction in the oriented polymer strip. The irreversible isomerization of the photoresponsive mesogens results in the synergistic phototunable bending and high-contrast fluorescence change. Based on the orthogonal responses to heat and light, controllable arm-like bending motions of this material, which is applicable in constructing advanced artificial muscles or intelligent soft robotics, are further demonstrated.

1. Introduction

Skeletal muscles are one of Nature's most incredible materials, capable of producing massive and precise deformations under the control of nervous systems. Various polymeric soft actuators, particularly those can change shape and convert external energy into mechanical functions, also known as artificial muscles, have been invented.[1–7] The investigations on artificial muscles have long focused on improving their mechanical performances.[8–10] Recently, there has been a growing trend in inventing artificial muscles with multiple stimuli-responses to enrich their applications,[11] or seeking approaches to make them more mechanically intelligent as to execute active and controllable deformations.[12,13] Integrating all these advantages in a polymeric system would offer the material fascinating prospects in applications such as human–machine interface, 3D display, or smart robotics.[14]

By sharing the anisotropic characteristics with skeletal muscles at both molecular and self-organization levels to some extent, liquid crystal polymers (LCPs) have been favored in constructing stimuli-responsive soft actuators, in addition to their light weight, adjustable modulus, and highly tunable chemical compositions. Wide ranges of artificial muscles are produced when mesogenic moieties are embedded into networks of chemical crosslinks, resulting in liquid crystal elastomers (LCEs) or liquid crystal networks, which can be actuated by numerous external stimuli such as heat,[3,9,10,15] light,[16–22] electric field,[23,24] magnetic field,[25,26] pH values,[27] or humidity.[28] The macroscopic deformation of these LCPs is primarily dependent on drastic changes in molecular conformation and orientation, which can be triggered by the phase transition between LC and isotropic state.[3,29] This deformation process is typically sharp and discontinuous, owing to the first-order phase transition. Skeletal muscles, on the other hand, can deform continuously in a controlled manner, relying on the collective motion of myofilaments inside the hierarchical cylindrical structure of muscle fiber bundles.[30,31]

LCP materials are inherent hierarchical in structure. As for LCPs with columnar phase, supramolecular cylinders bundle together parallelly to form LC domains. We suggest that through

Z. Yang, J. Li, X. Chen, Y. Fan, S. Yang, E.-Q. Chen
Beijing National Laboratory for Molecular Sciences
Key Laboratory of Polymer Chemistry and Physics of Ministry of Education
Center for Soft Matter Science and Engineering
College of Chemistry and Molecular Engineering
Peking University
Beijing 100871, P. R. China
E-mail: shuangyang@pku.edu.cn; eqchen@pku.edu.cn

J. Huang
Key Laboratory of Bioinspired Smart Interfacial Science and Technology of Ministry of Education
School of Chemistry
Beihang University
Beijing 100871, P. R. China

H. Yu
School of Materials Science and Engineering
Key Laboratory of Polymer Chemistry and Physics of Ministry of Education
Peking University
Beijing 100871, P. R. China

The ORCID identification number(s) for the author(s) of this article can be found under https://doi.org/10.1002/adma.202211648.
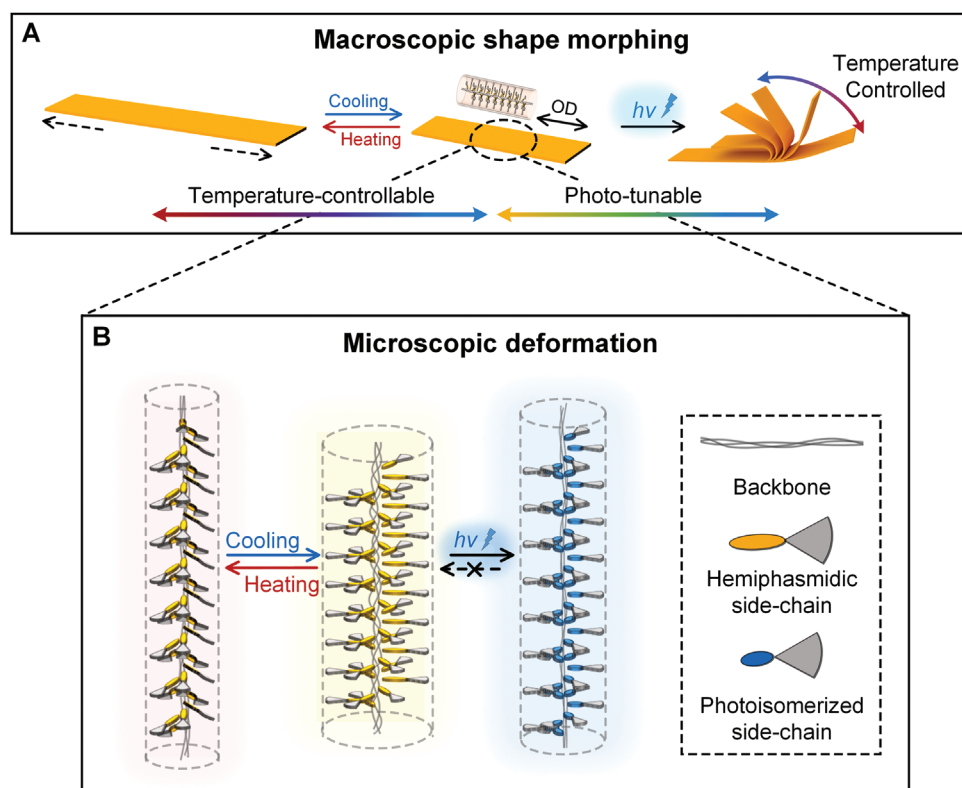
Scheme 1. Illustration of the hemiphasmidic SCLCP-based artificial muscle. A) Schematic macroscopic temperature-controlled and phototunable shape morphing of the muscle-like polymer strip. B) Schematic of microscopic thermally responsive and photoresponsive deformation of the multichain columnar assembly. The OD of the columnar assembly is parallel to the long axis of the strip.

regulating the microscopic deformation of individual cylindrical assembly, macroscopic controllable shape morphing can be obtained when the LC domains are well aligned. Assuming cylinders or columns in a columnar phase can shrink/expand the diameter in response to external stimuli, such a lateral "breathing" motion may transform to a continuous elongation/contraction along the columnar axis when the columnar phase is preserved (**Scheme 1**A). As artificial muscles based on columnar LCPs were rarely reported,[29,32,33] here we intend to demonstrate that both continuous and precisely regulated deformation can be achieved, using a hemiphasmidic side-chain LCP (SCLCP). With the side-chain comprising a rod-like mesogen in series with a bulky fan-like tail group, the hemiphasmidic SCLCP renders columnar phases, taking a unique multichain supramolecular column as the elementary building block (Scheme 1B). The multichain column has a "core–shell–corona" structure,[34–36] with several polymer backbones intertwined in the core. Tethered on the backbones are the wedge-shaped side-chains, of which the rod and fan form the shell and the corona part, respectively. As temperature increases, the expanding dynamic free volume of the shell and corona parts may squeeze the soft backbone core, resulting in entropy-driven sliding of backbones along the columnar axis, and thus a significant negative thermal expansion of the columnar lattice (Scheme 1B), rendering the material a thermally responsive artificial muscle. Furthermore, we will show that a careful selection of functional side-chain mesogens can endow the hemiphasmidic SCLCP with additional orthogonal stimuli-responses.

In the present work, the multichain column that can perform lateral "breathing" motion is based on the hemiphasmidic SCLCP bearing polycyclooctene as the backbone and dicyanodistyrylstilbenzene (DCS) as the rod-like mesogen (P-DCS12, see **Figure 1**A). In its hexagonal columnar phase (Φ_H), a tremendous negative thermal expansion of the hexagonal lattice is observed. The uniaxially aligned P-DCS12 strip shows a temperature-dependent and reversible linear elongation up to 118%, comparable to that of the real skeletal muscles. The DCS mesogen further makes P-DCS12 photoresponsive. When exposed to blue light, the strip can bend up to 180° and simultaneously display a sharp fluorescent color change from yellow to sapphire. Interestingly, the bending angle can be precisely programmed by adjusting the irradiation time. Moreover, the bent strip can vary its angle almost linearly with temperature, making the artificial muscle quantitatively temperature-controllable. This hemiphasmidic SCLCP-based actuator can thus be used in diverse aspects, including the vivid photo-painted architectures, two-way/one-way shape-memorial materials, and particularly, soft artificial arm that works on demand.

2. Results

2.1. Multichain Supramolecular Columns and Their Negative Thermal Expansion

The chemical structure of P-DCS12 is shown in Figure 1A. P-DSC12 was synthesized through the ring-opening metathesis
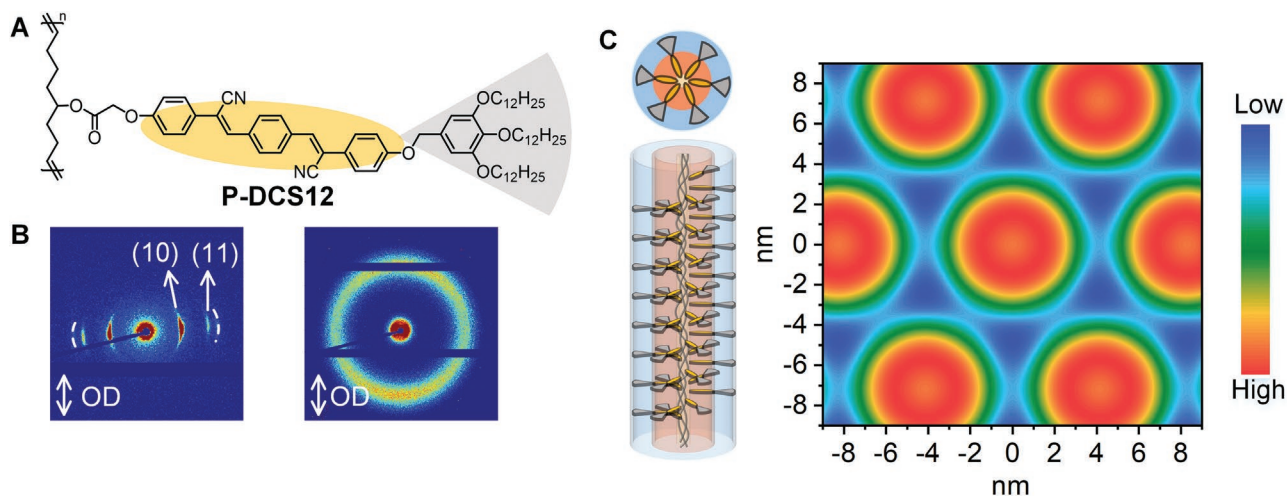
Figure 1. Characterization of the multichain supramolecular column phase. A) The chemical structure of P-DCS12. B) 2D XRD pattern of the oriented P-DCS12 strip. Left: Small-angle 2D XRD pattern, evidencing the typical diffractions of the columnar phase. Right: Wide-angle 2D XRD pattern showing side-chain mesogens aligned preferentially perpendicular to the OD. C) Schematic illustration (left) and reconstructed relative electron density map (right) of the supramolecular multichain columnar phase of P-DCS12. The color from blue to red represents the electron density from low to high.

polymerization method, of which the apparent number-average molecular weight was measured to be 1.4×10^5 g mol^{-1} using gel permeation chromatography calibrated with polystyrene standards. Well-oriented P-DCS12 strips were then readily obtained by simple compressing which forced the polymer to flow along the longitudinal direction in a thin rectangular mold (Figure S2A, Supporting Information).

The 2D X-ray diffraction (2D XRD) pattern of the uniaxially aligned P-DCS12 strip exhibits typical hexagonal diffractions perpendicular to the orientation direction (Figure 1B). Giving the small angle diffractions with the q-ratio of $1:\sqrt{3}:\sqrt{4}$ ($q = 4\pi\sin\theta/\lambda$), the hexagonal lattice parameter a of 8.3 nm is identified for the Φ_H phase. Meanwhile, the high angle scattering concentrating on the orientation direction (OD, the meridian) at 0.44 nm suggests a preferential packing of side-chains perpendicular to the columnar axis (Figure 1B). Assuming 0.44 nm the c parameter of the hexagonal unit cell, the number of repeating units (Z_{rep}) packed in a unit cell is estimated to be 16, using the expression $Z_{rep} = (N_A/M)(a^2 c\sin60°)\rho$, with N_A the Avogadro's number, M the molar mass of repeating unit, and ρ the density of P-DCS12 (1.03 g cm^{-3} as measured). Such a large Z_{rep} indicates that there are several polymer chains incorporated together to fulfill the unit cell, which gives rise the formation of a multichain supramolecular column.[36–38] The reconstructed 2D relative electron density map (EDM, Figure 1C) of the Φ_H phase presents the "core–shell–corona" structure, where the core consists of preferentially polycyclooctene backbones with the middle electron density, surrounded by a shell of the aromatic DCS mesogens and the corona of tails.

The multichain columnar structure endows P-DCS12 with unique LC phase behavior as well as mechanical property. In addition to the glass transition temperature (T_g) of 45 °C, the differential scanning calorimetry (DSC) measurement indicates the isotropic temperature (T_i) at 188 °C (Figure S3A, Supporting Information). The polarized optical microscopy experiments further reveal that at T_i there is a Φ_H-isotropic transition (Figure S3B,C, Supporting Information). While the

in situ thermal XRD measurement proves that P-DCS12 always remains in its Φ_H phase below T_i, the rheology temperature sweep experiment reveals that its mechanical property drastically changes. Along with the glass transition, the modulus of P-DCS12 declines until 80 °C and then reaches the plateau of rubbery state (**Figure 2**A). Consequently, we suggest that the Φ_H phase could be divided into three stages: 1) the "frozen state" (below T_g, the columnar assemblies are rigid); 2) the "transition zone" (T_g to 80 °C, relaxation of chain segment occurs); and 3) the "soft state" (above 80 °C, chain movements are active and the columnar assemblies are in fact supersoft).

We notice that in the "frozen state," the hexagonal diffractions of P-DCS12 stay unchanged. When the strip was heated above its T_g to 150 °C, the diffractions continuously shift from $q = 0.87$ to 0.97 nm^{-1}, which can then fully recover to the original state during the cooling process (Figure S4, Supporting Information). The pronounced shifted diffractions evidence the continuous and reversible change of the lattice parameter a, unveiling an unusual negative thermal expansion. Similar results have also been observed in molecules based on tapered monodendritic moieties that self-assemble into columnar phases.[32,39,40] According to Ungar et al., the lateral shrinkage of columns with increasing temperature is due to the rejections of the surplus molecules. Nevertheless, inside the multichain columnar assembly of P-DCS12, long chains shall be strongly intertwined, preventing chains from being expelled from the column. At higher temperatures, the side-chain scattering diffuses in azimuth distribution (Figure S5, Supporting Information), indicating that the side-chains become more inclined rather than perpendicular to the columnar axis. We deduce that the strengthened thermal motion of side-chains at higher temperatures accounts for the column shrinkage. Because the side-chains tethered to the backbone swing and take up more dynamic free volume, a larger interfacial area between the "core" and "shell" is required, and thus the curvature of the core has to increase. In this case, the fiercer the side-chain motion, the more the core occupied by the backbones

**ADVANCED
SCIENCE NEWS**

www.advancedsciencenews.com

**ADVANCED
MATERIALS**

www.advmat.de
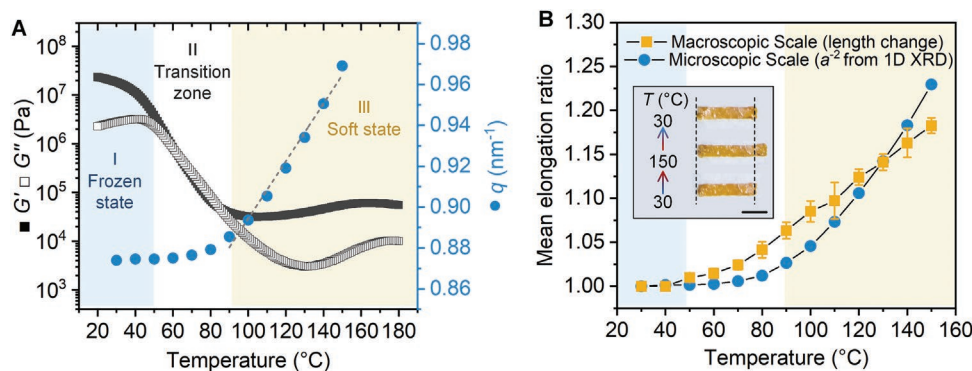
Figure 2. Liquid crystal phase behavior and mechanical properties of P-DCS12. A) Demonstration of the three regions of polymer chain movements. The storage and loss shear modulus (G' and G'') were measured by rheology temperature sweep experiment. The values of q corresponding to the (10) plane of the Φ_H phase were determined by a thermal XRD experiment. B) Elongation ratio of the P-DCS12 strip (yellow square) as a function of temperature during heating process. For comparison, the ratio of $[a(T)/a(T = 30\ °C)]^{-2}$ (blue circle) is also plotted, where a is the hexagonal lattice parameter obtained from thermal 1D XRD. Inset: photos that show the reversible elongation of the strip. Scale bar: 5 mm.

is squeezed. This idea is supported by the EDM result of P-DCS12 at 150 °C (Figure S6, Supporting Information). It is worth noting that the polycyclooctene backbones of P-DCS12, with an average graft density of 1 side-chain per 7 backbone carbon atoms, is quite flexible and can submit to the enhanced motion of the side-chains. Once the core area is reduced, the backbones would begin to elongate along the columnar axis together with the tethered side-chains. The dimension variation is fully reversible, vividly demonstrating the unique "breathing" motion of the columnar assemblies in P-DCS12.

2.2. Thermally Responsive Muscle-Like Elongation/Contraction

The negative thermal expansion of columns is inherent for the Φ_H phase of P-DCS12. However, the transform of microscopic "breathing" motion into macroscopic deformation requires ordered packing of columnar assemblies. In the uniaxially aligned P-DCS12 strip, we found that the above-mentioned negative thermal expansion in an individual multichain column could be well exaggerated into muscle-like elongation/contraction of the strip (Figure S7, Supporting Information). The sample experiences spontaneous elongation upon heating to above T_g; when heated to 150 °C, the elongation ratio was detected to be 118% (Figure 2B). Such an elongation is comparable to real muscle fibers, which is less than 120%.[41,42]

It is clear that the strip elongation is well correlated with the shrinkage of the multichain columns. From the perspective of geometry, the following function gives the relationship between the hexagonal lattice parameter (a), length (L_{col}), and volume (V_{col}) of a single Φ_H phase domain: $L_{col} = 4V_{col}/a^2 \sin 60°$. Assuming that the density (ρ) and the volume (V_{col}) of the given polymer remain constant, one has $L_{col} \propto a^{-2}$ in a uniaxially aligned material. Since the positive bulk thermal expansion of polymeric materials is inevitable, the theoretical prediction of $L_{col} \propto a^{-2}$ only gives the low limit of length increase due to the columnar lattice's negative thermal expansion. Furthermore, because of fiercer side-chain fluctuation and partial relaxation of orientation at higher temperatures, the elongation ratio becomes slightly lower than the predicted value.

2.3. Photoinduced Deformation and Fluorescent Change

As a derivative of α-cyanostilbenes, DCS bears the aggregation-induced emission enhancement feature[43–46] and can undergo photochemical reactions when being exposed to light stimulus.[47–51] Under the irradiation of visible light at 450 nm, the structural changes of DCS cores of the monomer M-DCS12 and the polymer P-DCS12 were tracked by ^{1}H NMR spectroscopy in their solutions (Figure S8A,B, Supporting Information). A typical signal at 8.2 ppm, depicting the protons on the central phenyl-rings in the Z,Z-DCS isomer, completely disappeared after a continuous irradiation of 12 h, indicating that the Z,Z-isomers were all consumed. Accordingly, blue shifts of the UV-Vis absorption and emission peaks were detected from the spin-coated transparent P-DCS12 films, suggesting that the resulting products exhibited reduced conjugation extents and widened energy gaps between their highest occupied molecular orbitals and lowest unoccupied molecular orbitals (**Figure 3**A). This may be ascribed to the formation of the E,Z- (Z,E-) or E,E-isomers (Figure S9, Supporting Information). Besides, it was found that the irradiated P-DCS12 strips could only be partially dissolved in organic solvents (Figure S8C, Supporting Information), which may indicate the occurrence of an additional [2+2] cycloaddition between mesogens in bulk state,[52,53] leading to chemical crosslinks in the columnar assembly of P-DCS12. The possible crosslinking was also inferred from the atomic force microscopy observation. Compared with the unirradiated one, the surface of columnar assembly becomes rough and more undulated, which may be associated with the crosslinks generated inside/between the columns (Figure S8D,E, Supporting Information). The products from the photochemical reactions (Figure 3B) were rather stable (Figure S10, Supporting Information), making the variation of chemical structures irreversible.

Intriguingly, the P-DCS12 strip responded to blue light with not only fluorescent changes but also bending motions. The emission color changed from yellow to sapphire over a huge wavelength range of 80 nm. When irradiated at room temperature, the uniaxially aligned P-DCS12 strip could quickly bend away from the light source, reaching a bending angle of 180° within 50 s (**Figure 4**A and Movie S1, Supporting Information).
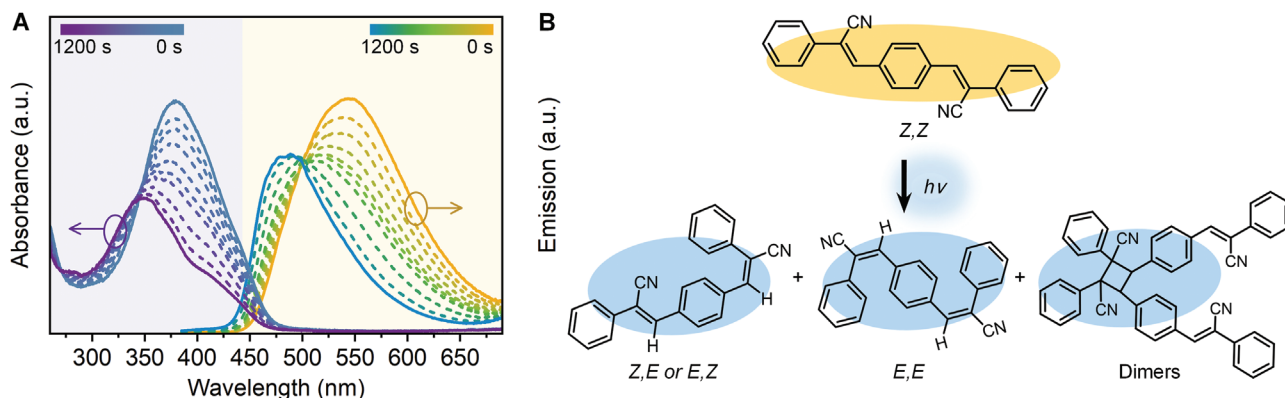
Figure 3. Photochemical changes of P-DCS12. A) The UV–Vis (left) and photoluminescent (right) spectra of the spin-coated transparent P-DCS12 film recorded during continuous irradiation of 450 nm light. Both the absorption and emission blue shift with increasing irradiation time. B) Possible structural changes of DCS moiety. Only part of the possible products is presented here. Other products such as *E,Z*-dimer or *E,E*-dimer are omitted due to the lack of space.

Through selective irradiation, these two features, i.e., photochromism and photodeformation, could be combined to create a variety of vivid architectures with high-contrast fluorescence (Figure 4B).

To deliberate the mechanism of bending motion during photoactuation, we used XRD measurements to track changes in the Φ_H phase (**Figure 5**A). Despite the dramatic chemical structure modifications of the DCS moiety, P-DCS12 sustains the columnar LC phase with hexagonal symmetry, indicating the robust self-assembly of multichain columns (Figure 5A). Furthermore, as the photochemical reactions proceeded, the hexagonal diffractions gradually shifted to higher angles. After prolonged irradiation, the (10) diffraction stabilized at q of 0.98 nm^{-1}, corresponding to a of 7.4 nm, which is 0.9 nm smaller than that of the unirradiated P-DCS12. This shrinkage is consistent with DCS moieties' chemical structural variation (Figure S9B, Supporting Information). As the XRD results confirmed the integrity of the multichain columnar assemblies, we anticipate that the blue light can drive elongation of the multichain column. When only one side of a uniaxially aligned strip is exposed to light, such a column elongation can cause the strip to bend, as depicted in Figure 4B.

2.4. Light-Programmable, Temperature-Controllable Bending

Integrating the "breathing" motion of supramolecular columns and the photoinduced irreversible chemical modification, P-DCS12 is a fascinating smart material. For the uniaxially aligned P-DCS12 strip, bending can be spatially located at the area shined by blue light. Importantly, the bending angle (θ) can be precisely programmed by tuning the irradiation time (t). For the bent strip, this angle can be further dynamically controlled by varying environmental temperature (T). At room temperature, we measured the bending angles of the P-DCS12 strip at different exposure times. Figure S11 in the Supporting Information presents the experimental details, in which we carefully avoided the photothermal effect (Figure S12, Supporting Information). The bending angle gradually increased with irradiation time, eventually reached 180° when the strip folded as a hairpin (**Figure 6**A). We then set a 180°-bent P-DCS12 strip at different temperatures to investigate the relationship between the bending angle and temperature (Figure 6B). The strip almost remained unchanged in its "frozen state" and began to unfold at around 60 °C. Then it gradually opened up to nearly flat, with a bending angle of 19° at 150 °C (Figure S13, Supporting Information). It is worth mentioning that the hairpin-like strip unfolded quickly, and the equilibrium bending angle at each temperature was reached in seconds. As shown in Figure 6B, a linear relationship is discovered in the "soft state" of P-DCS12, making the P-DCS12 strip a "protractor" styled temperature gauge (Figure 6B).

The bend morphing shall be associated with the P-DCS12 strip's heterogenous structure. We examined the Φ_H phase and rheological properties of the fully irradiated P-DCS12 strip to explore the mechanism of the controllable bending movements. As aforementioned, blue light irradiation can cause the multichain columns to shrink. Thermal XRD experiments
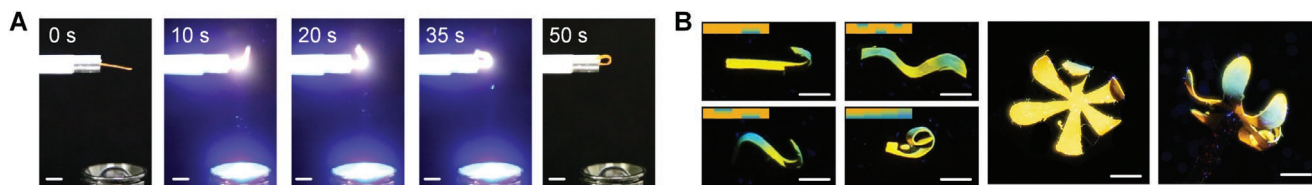
Figure 4. The photochromism and photodeformation of P-DCS12 with irradiation of blue light. A) Visual demonstration of the photoinduced bending of P-DCS12 strip. When shining blue light on the low side of the strip, the strip bends upward and fully folds within 50 s. Scale bar: 5 mm. B) Various architectures with high-contrast fluorescent color under UV light, which were constructed upon irradiations on selective area. Scale bar: 3 mm.

**ADVANCED
SCIENCE NEWS**

www.advancedsciencenews.com

**ADVANCED
MATERIALS**

www.advmat.de
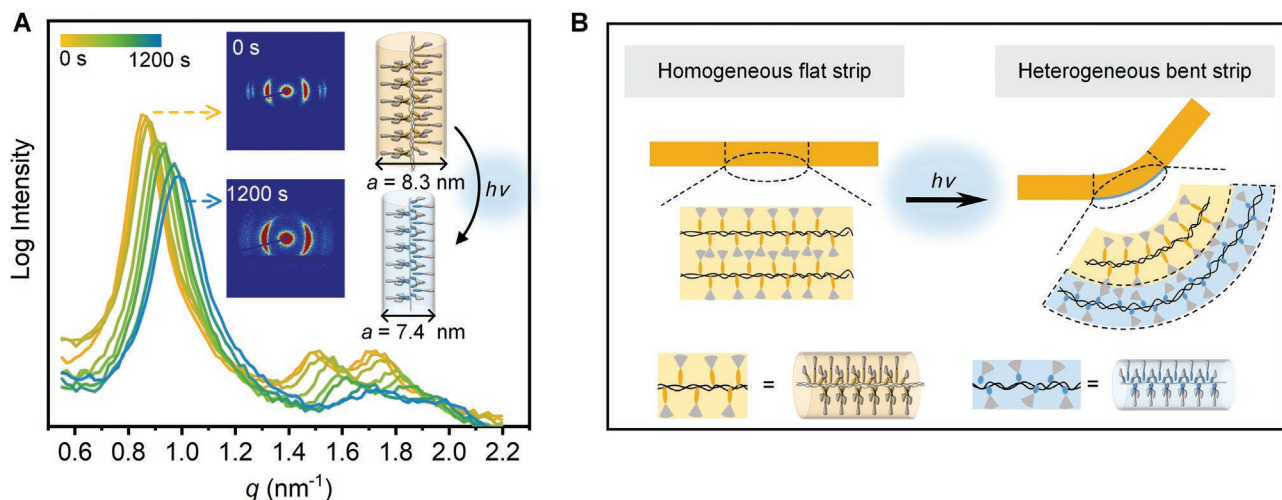
Figure 5. The photoinduced deformation of the multichain columnar assemblies. A) 1D XRD results present the shifts of diffraction peaks with increasing irradiation time from 0 to 1200 s. Inset: Left: 2D XRD patterns before and after irradiation, demonstrating the intact of the columnar assembly. Right: illustration of the shrinkage of the multichain columnar assembly caused by light illumination. B) Schematic illustration of the photoinduced bending of the P-DCS12 strip, wherein the side exposed to light expands along the longitudinal direction of the strip due to the lateral shrinking of irradiated columns.

show that the hexagonal lattice in the irradiated strip has only a negligible positive thermal expansion, distinctly different from the unirradiated ones (Figure 6C). Additionally, while the virgin P-DCS12 is supersoft at temperatures above 80 °C, irradiation stiffened the polymer, increasing the storage modules of P-DCS12 by an order of magnitude (Figure 6C), which might be ascribed to the crosslinks formed via the [2+2] cycloaddition of adjacent DCS molecules inside the columns (Figure S14, Supporting Information). Based on these findings, we presume that the light penetration depth, which extends with irradiation time, determines the bending angle of a single side-irradiated strip at a constant temperature. In this case, using blue light, a heterogenous structure containing the bending information can be written into the P-DCS12 strip.

We propose a simplified bilayer model to further understand the controlled bending. The programmed P-DCS12 film, in particular, is made up of two layers: the unirradiated and the irradiated one (i.e., the upper and lower layers shown in Figure 5B). These two layers differ with each other in both the thermal expansion coefficient and the storage modulus G' (Figure 6C). In the "soft state," the upper layer can be regarded as a softer elastic plate, while the lower layer the stiffer one. For a folded strip, as temperature rises, the upper layer elongates significantly, driving the strip to unfold. Nonetheless, the lower layer with higher G' supports the entire strip and attempts to maintain the bending angle. Geometrically, the length difference between two layers determines the equilibrium bending angle θ, as depicted in Figure S15 in the Supporting Information. Based on the bilayer model, the energy argument can give the expression of the equilibrium bending angle θ

$$\theta = \frac{180}{\pi} \frac{4L_0}{d_1} \varepsilon(T) \frac{1 - \varepsilon(T)}{\frac{E_1 d_1}{3E_2 d_2} + (1 - \varepsilon(T))} \tag{1}$$
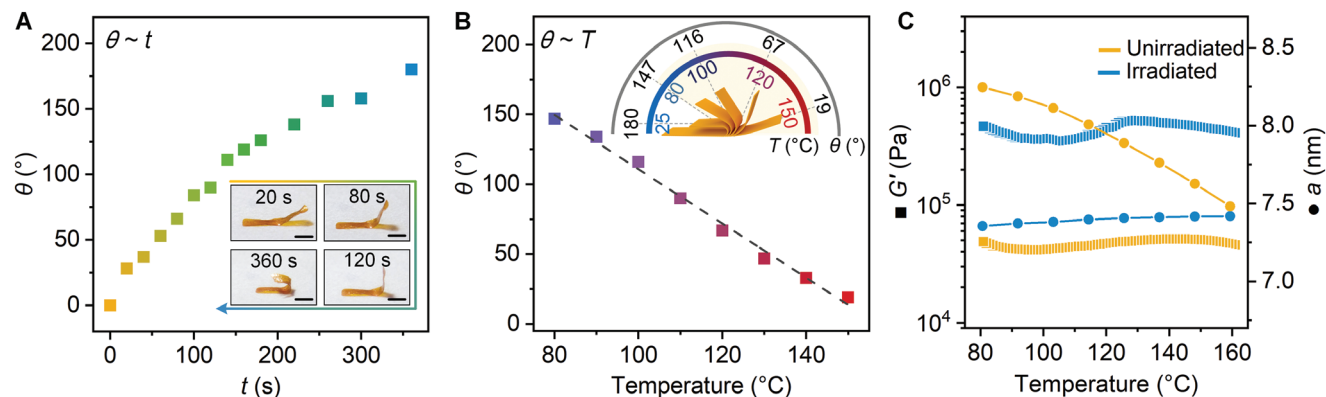
Figure 6. Precisely photoprogrammable and temperature-controllable bending. A) Plot of the bending angle θ to the irradiation time t. Inset: Photos presenting the irradiation-time-adjustable bending. Scale bar: 3 mm. B) Linear change of the equilibrium bending angle with temperature. The strip used for the measurement was 180°-folded at room temperature. Inset: Schematic illustration of the "protractor" styled "temperature gauge." C) Changes of the hexagonal lattice parameter a and the storage modulus G' of P-DCS12 before and after irradiation in the "soft state" from 80 to 150 °C.

**ADVANCED
SCIENCE NEWS**

www.advancedsciencenews.com

**ADVANCED
MATERIALS**

www.advmat.de

where L_0 is the length of the strip at 160 °C; d_1 and E_1, respectively, are the thickness and storage modulus of the unirradiated layer, and d_2 and E_2 of the irradiated layer; $\varepsilon(T)$ is strain of contraction of the unirradiated layer at a given temperature, which is experimentally determined as: $\varepsilon(T) = 0.0016 \times (160 - T)$. Specifically, as $\varepsilon(T)$ is small, the last term in Equation (1) changes little and could be considered a constant. Therefore, there is a scaling as $\theta \sim \varepsilon(T) \sim -T$, which is consistent with the experimental results shown in Figure 6B. Equation (1) also indicates that the bending angle is inversely proportional to d_1. For a strip with a constant thickness of $d = d_1 + d_2$, it in fact suggests $\theta \sim d_2$. Therefore, the increment of θ with lengthening the irradiation time t (Figure 6A) is due to the gradually thickened irradiated layer. Detailed deduction and calculations are provided in the Supporting Information. Based on the data achieved in experiments, the bending angles can be calculated quantitatively using Equation (1) (Figure S16, Supporting Information). All the calculated results fit the experimental ones very well, indicating that the bending motion of the P-DCS12 strip can indeed be precisely controlled (Figure 6A,B).

2.5. Shape-Memory Property and Object Lifting Ability

Genuinely, when temperature exceeds its T_g, the uniaxially aligned P-DCS12 is a two-way shape-memory material, which can execute reversibly the continuous elongation/contraction or folding/unfolding. Using of the "frozen" Φ_H phase, we can impose an additional one-way shape memory to P-DCS12. The shape distortion of the P-DCS12 strip was carried out with external force at 80 °C. Diverse temporary shapes such as flattened, twisted, folded, and curled strips were readily fixed by quenching the polymer to room temperature (Figure S17, Supporting Information). For the light-programmed bent strip, fabricating the temporary shapes did not destroy its heterogenous structure. The shape recovery process was then carried out on-demand by heating the strip to any temperature within the "soft state" and it would achieve its permanent shape with the equilibrium bending angle defined by the temperature. Further varying temperature led the bending angle to change in concert,

corresponding to that presented in Figure 6B (Figure S13, Supporting Information).

The heterogenous structure programmed in P-DCS12 by local photochemical reactions can also serve as a hinge point, similar to human elbows. The P-DCS12 strip thus can be regarded as an "artificial arm" We tested the performance of the "artificial arm" with a 180°-bent strip, of which the "hinge" of a 1.5 mm width was prepared by light irradiation through a photo mask. When the strip became sticky due to its low G' at 120 °C, we attached an object to the edge of the strip, 2 mm away from the "hinge." The strip began to lift the object as it was gradually cooled to the temperature range of the "transition zone." As the temperature lowered, the object was raised to a higher position (**Figure 7**A and Figure S18, Supporting Information).

As previously discussed, both the backbones and side-chains are highly activated in the "soft state," and the storage modulus G' is rather low ($\approx 3 \times 10^4$ Pa). However, the multichain columns' vitrification occurs when they enter the "transition zone." As a result, the G' of the unirradiated layer can finally rise to $\approx 10^7$ Pa, which is three orders of magnitude higher than that of the "soft state" (Figure 2A). The G' of the irradiated part, on the other hand, increases slightly with decreasing temperature (Figure 7B). Presumably, the kinked DCS isomers (e.g., E,Z- or E,E-isomers) and the chemical crosslinks between mesogens in the columns can retain their loss of packing and mobility to a certain extent at low temperatures. Notably, while the irradiated part remains largely unchanged both structurally and mechanically, the object lifting appearing within the "transition zone" shall be attributed primarily to the improved mechanical strength of the unirradiated layer. Consequently, the bending angle of the artificial arm follows a well-consistent trend with the climbing G' of the virgin P-DCS12 (Figure 7B). In this P-DCS12 strip, only the part subjected to one-sided irradiation produces the required work for lifting the object. That is, the P-DCS12 strip weighed 0.31 mg is strong enough to lift an object more than 30 times its own weight (10.5 mg, Figure S18, Supporting Information). Due to the complexity of the working system, the actual work density is difficult to calculate. As an alternative, we discussed the maximum output work in Supporting Information using the previous bilayer model (Figure S19, Supporting Information).
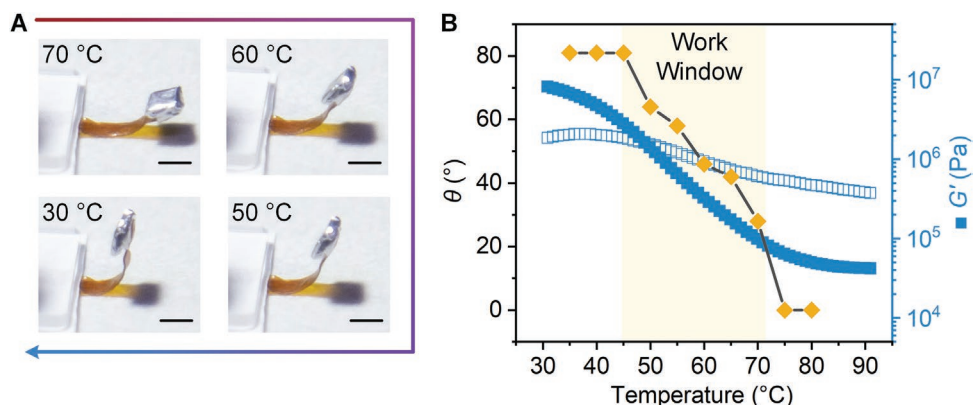
Figure 7. Temperature-controlled object lifting. A) Visual demonstration of the temperature-controlled lifting of the object. The heavy load attached at the end of the strip is nearly 30 times the weight of the irradiated part of the P-DCS12 strip. Scale bar: 3 mm. B) Comparison between the strip's bending angle and the storage shear modulus during the cooling process. The filled diamond refers to bending angle θ, the filled square refers to G' before irradiation while the open one for G' after irradiation.

**ADVANCED
SCIENCE NEWS**

www.advancedsciencenews.com

**ADVANCED
MATERIALS**

www.advmat.de

3. Discussion

The artificial muscle of P-DCS12 reported in this paper is unique compared to conventional LCE-based materials. Not only can the contraction and bending motions of human muscles be successfully imitated, but the shape morphing can also be precisely controlled. The outstanding performance of this hemiphasmidic SCLCP is based on the fact that the orthogonal responses to heat and light are inherently integrated through the self-assembled multichain supramolecular column.

The key mechanism applied to build the artificial muscle of P-DCS12 is the "breathing" motion of columns that can be converted into the continuous elongation/contraction. During the "breathing" process, the adaptable chain conformation in the persistent columnar assembly becomes critical, and the regulation of cooperative motions of the backbone and side-chain is required. For traditional LCEs, when the mesogen orientation is disrupted, they experience large-scale chain corruption, which invokes the order–disorder phase transitions. On the contrary, in the hemiphasmidic SCLCP of P-DCS12, positional reorganizations between the elastic backbone and rigid side-chains can be realized without destroying the overall LC phase structure. We select polycyclooctene as the main chain so that the side-chain density is much lower than that of conventional SCLCPs (i.e., polyacrylate). The backbone interval between the two adjacent side-chains is rather flexible, which can adjust its conformations properly to accommodate the enhanced side-chain motions when temperature is increased. As discussed before, this cooperativity leads to a tremendous negative thermal expansion of the columnar lattice. However, if hemiphasmidic SCLCPs have relatively stiffer backbones, such behavior was restricted.[37,38]

To impart more stimulated responsiveness to the artificial muscle, the characteristic of mesogen also matters. The most widely used photoresponsive moieties are azobenzene and its derivatives, which endow soft actuators with extraordinary features such as reversible deformation, short response time (a few seconds), and unique self-oscillation behavior.[16,20,22] Despite these merits, the short lifetime of *cis*-azobenzene isomers makes such deformations lack thermal stability, the durability of an on-demand deformed shape is reduced and thus may limit their further applications in soft robotics or machines.[20] Here in P-DCS12, the photochemical reaction of DCS moiety provides irreversible structural changes. Accordingly, not only could the photochromic P-DCS12 be used as the canvas for photo-painting with bright and high-contrast colors, but permanent bio-mimetic architectures could be fabricated using light. The photo-written local heterogenous structure is a thermal-stable hinge point that acts as the human elbow, directing the bending motions of the P-DCS12 strip as an artificial arm. Taking advantage of the climbing modulus caused by the vitrification of multichain columns, the artificial arms can lift objects much heavier than their own weight.

The extraordinary feature of P-DCS12 is the precise photoprogrammability and temperature-controllability, which are rare in conventional azobenzene-based actuators that often have nonnegligible photothermal effect.[54–56] In P-DCS12, the structural change of DCS moieties under blue light takes place much slower than that of azobenzenes, which might be ascribed to a lower extinction coefficient of DCS moiety at 450 nm (Figure S20, Supporting Information, $\approx 3.6 \times 10^2$ L mol^{-1} cm^{-1} vs $\approx 2 \times 10^4$ L mol^{-1} cm^{-1} for azobenzenes at 365 nm).[57,58] The relatively weak absorption allows the regulable penetration of blue light and thus the photoprogrammable bending. It is also vital that the Φ_H phase of the P-DCS12 presents orthogonal responses to light and heat, making the quantitative control of the deformation possible. Consequently, the uniaxially aligned P-DCS12 strip works as the "thermal-meter" which exhibits immediate and accurate response to environmental temperature.

It is worth pointing out that toward the artificial muscle with the continuous morphing ability, the photoresponsiveness is not the first to be concerned, though we take advantage of DCS mesogen to fabricate the artificial muscle in a single polymer system. The main mechanism is the "breathing" motion of supramolecular columns, which can be encountered in other molecules.[29,32,33,39,40] When such columns are combined with other materials of normal thermal expansion to construct a heterogenous structure (e.g., bilayer), the device will be able to bend when changing temperature and work as an artificial arm. Moreover, according to Equation (1), a relationship between equilibrium bending angle θ and all other experimental parameters is obtained. Therefore, the method we report here can represent a general strategy for the construction of the artificial arm, irrespective of the special molecular structure.

In conclusion, we have demonstrated a novel hemiphasmidic SCLCP, P-DCS12, that can self-assemble into a multichain supramolecular columnar phase with the unique "breathing" motion, leading to the extraordinary negative thermal expansion of its columnar lattice. P-DCS12 imitates skeleton muscles in many ways: the hierarchical columnar structure, the continuous elongation/contraction motions, the ability to output work, and most incredibly, the precise and quantitative controllability with external stimuli of light and heat. On the other hand, as can perform reversible elongation/contraction, P-DCS12 differs from skeleton muscles that can contract only. Thus, we highlight that the "breathing" motion of the multichain columns with flexible long chain as the backbone is powerful for inventing thermally responsive soft actuators. Furthermore, the photoresponsive mesogen in P-DCS12 allows the heterogenous structure to be spatially patterned using light. With layered heterogenous structures, a small contraction can turn to be sharp bending, resulting in a lifting of heavy loads. The temperature-defined columnar phase behavior shows superiority in the precise control of the dynamic motions of the obtained material. In view of the demand of diversity for developing polymeric materials, we anticipate such hemiphasmidic SCLCP and other polymers of columnar phases, with variable compositions, easy-obtained orientation, strengthened mechanical strength, and good processability, can serve as a novel and substantial platform for advanced soft actuators.

4. Experimental Section

Synthesis and Polymerization of P-DCS12: The synthetic route of the monomer M-DCS12 is provided in the Supporting Information. P-DCS12 was polymerized through the ring-opening metathesis polymerization method from its monomer M-DCS12.

NMR Spectrum: The *Z,Z*-configuration of the monomer M-DCS12 was confirmed by 1D rotating frame overhause effect spectroscopy (600 MHz, CDCl$_3$) spectrum of M-DCS12. The spinlock time was set to 200 ms. ROE% = 4.6%.

Preparation of the Uniaxially Aligned P-DCS12 Strips: P-DCS12 doped with a tiny amount of paraffin oil (less than 5 wt%) was used to fabricate the uniaxially oriented strip. Adding a little of paraffin oil could help to dissipate internal stress generated between well-developed LC domains and thus to obtain intact films with better flexibility and robustness. P-DCS12 doped with paraffin oil was annealed at 110 °C for 30 min for Φ_H phase cultivation. After that, the sample was forced to flow along the longitudinal direction in a thin sample cell (15 mm × 2 mm, 100 μm in thickness) at 110 °C with 4 MPa external pressure held for 10 s to achieve uniaxial orientation. Both the shape and alignment were fixed through quenching. Schematic illustration of the preparation and the 2D XRD patterns proving the uniaxial alignment is shown in Figure S2 in the Supporting Information.

Measurement of the Relationship between Irradiation Time t and Bending Angle θ: In order to explore the relationship between the irradiation time *t* and the bending angle *θ*, the blue light was put farther to reduce the power of light and weaken the influence of photo-thermal effect. For the light-to-sample distance (4 cm) which was set for the experiment, only a slight temperature increase was detected after the irradiation of 10 min (Figure S12, Supporting Information). As shown by Figure S11 in the Supporting Information, the P-DCS12 strip was attached to the table to keep flat throughout the irradiation process. Both ends of the strip were shaded with masks and only the middle part (4.0 mm in length) was exposed to the blue light. After being irradiated for some time, the flat strip with the light-written structure was annealed at 100 °C for 1 min in order to activate the chain motion and remove all the unexpected internal stress produced by the columnar deformation induced by the irradiation process. After annealing, the P-DCS12 strip was cooled down to room temperature and a bending shape was achieved. The bending angle was measured at room temperature. Different irradiation times were resulted in different bending angles.

Supporting Information

Supporting Information is available from the Wiley Online Library or from the author.

Acknowledgements

Conflict of Interest

The authors declare no conflict of interest.

Data Availability Statement

The data that support the findings of this study are available from the corresponding author upon reasonable request.

Keywords

[1] T. Mirfakhrai, J. D. W. Madden, R. H. Baughman, *Mater. Today* **2007**, *10*, 30.

[2] Y. Takashima, S. Hatanaka, M. Otsubo, M. Nakahata, T. Kakuta, A. Hashidzume, H. Yamaguchi, A. Harada, *Nat. Commun.* **2012**, *3*, 1270.

[3] M.-H. Li, P. Keller, *Philos. Trans. R. Soc., A* **2006**, *364*, 2763.

[4] J. M. McCracken, B. R. Donovan, T. J. White, *Adv. Mater.* **2020**, *32*, 1906564.

[5] C. Greco, P. Kotak, L. Pagnotta, C. Lamuta, *Int. Mater. Rev.* **2022**, *67*, 575.

[6] B. Jin, H. Song, R. Jiang, J. Song, Q. Zhao, T. Xie, *Sci. Adv.* **2018**, *4*, eaao3865.

[7] Y. Wu, Y. Yang, X. Qian, Q. Chen, Y. Wei, Y. Ji, *Angew. Chem., Int. Ed.* **2020**, *132*, 4808.

[8] J. Sun, Y. Wang, W. Liao, Z. Yang, *Small* **2021**, *17*, 2103700.

[9] X. Pang, J. Lv, C. Zhu, L. Qin, Y. Yu, *Adv. Mater.* **2019**, *31*, 1904224.

[10] H.-F. Lu, M. Wang, X.-M. Chen, B.-P. Lin, H. Yang, *J. Am. Chem. Soc.* **2019**, *141*, 14364.

[11] Z. Li, P. Liu, X. Ji, J. Gong, Y. Hu, W. Wu, X. Wang, H.-Q. Peng, R. T. K. Kwok, J. W. Y. Lam, J. Lu, B. Z. Tang, *Adv. Mater.* **2020**, *32*, 1906493.

[12] J. Wang, M.-F. Lin, S. Park, P. S. Lee, *Mater. Today* **2018**, *21*, 508.

[13] C. Ni, D. Chen, Y. Zhang, T. Xie, Q. Zhao, *Chem. Mater.* **2021**, *33*, 2046.

[14] J. Wang, D. Gao, P. S. Lee, *Adv. Mater.* **2020**, *33*, 2003088.

[15] D. L. Thomsen, P. Keller, J. Naciri, R. Pink, H. Jeon, D. Shenoy, B. R. Ratna, *Macromolecules* **2001**, *34*, 5868.

[16] J. Lv, Y. Liu, J. Wei, E. Chen, L. Qin, Y. Yu, *Nature* **2016**, *537*, 179.

[17] Y. Luo, Y. Guo, X. Gao, B.-G. Li, T. Xie, *Adv. Mater.* **2012**, *25*, 743.

[18] H. Zeng, P. Wasylczyk, C. Parmeggiani, D. Martella, M. Burresi, D. S. Wiersma, *Adv. Mater.* **2015**, *27*, 3883.

[19] J. Chen, F. K.-C. Leung, M. C. A. Stuart, T. Kajitani, T. Fukushima, E. van der Giessen, B. L. Feringa, *Nat. Chem.* **2017**, *10*, 132.

[20] M. Lahikainen, H. Zeng, A. Priimagi, *Nat. Commun.* **2018**, *9*, 4148.

[21] F. Lancia, A. Ryabchun, A.-D. Nguindjel, S. Kwangmettatam, N. Katsonis, *Nat. Commun.* **2019**, *10*, 4819.

[22] A. H. Gelebart, D. J. Mulder, M. Varga, A. Konya, G. Vantomme, E. W. Meijer, R. L. B. Selinger, D. J. Broer, *Nature* **2017**, *546*, 632.

[23] W. Lehmann, H. Skupin, C. Tolksdorf, E. Gebhard, R. Zentel, P. Krüger, M. Lösche, F. Kremer, *Nature* **2001**, *410*, 447.

[24] E. Acome, S. K. Mitchell, T. G. Morrissey, M. B. Emmett, C. Benjamin, M. King, M. Radakovitz, C. Keplinger, *Science* **2018**, *359*, 61.

[25] Y. Kim, H. Yuk, R. Zhao, S. A. Chester, X. Zhao, *Nature* **2018**, *558*, 274.

[26] Q. Ze, X. Kuang, S. Wu, J. Wong, S. M. Montgomery, R. Zhang, J. M. Kovitz, F. Yang, H. J. Qi, R. Zhao, *Adv. Mater.* **2019**, *32*, 1906657.

[27] W. Wang, X. Xu, C. Zhang, H. Huang, L. Zhu, K. Yue, M. Zhu, S. Yang, *Adv. Sci.* **2022**, *9*, 2105764.

[28] H. Arazoe, D. Miyajima, K. Akaike, F. Araoka, E. Sato, T. Hikima, M. Kawamoto, T. Aida, *Nat. Mater.* **2016**, *15*, 1084.

[29] V. Percec, J. G. Rudick, M. Peterca, P. A. Heiney, *J. Am. Chem. Soc.* **2008**, *130*, 7503.

[30] I. Agarkova, J.-C. Perriard, *Trends Cell Biol.* **2005**, *15*, 477.

[31] K. E. Davies, K. J. Nowak, *Nat. Rev. Mol. Cell Biol.* **2006**, *7*, 762.

[32] Y. K. Kwon, S. N. Chvalun, J. Blackwell, V. Percec, J. A. Heck, *Macromolecules* **1995**, *28*, 1552.

[33] J. Wang, X.-Q. Liu, X.-K. Ren, B. Zhang, S. Yang, F. Liu, B. Lotz, E.-Q. Chen, *Chem. – Asian J.* **2016**, *11*, 2387.

**ADVANCED
SCIENCE NEWS**

www.advancedsciencenews.com

**ADVANCED
MATERIALS**

www.advmat.de

[34] C. Lin, H. Ringsdorf, M. Ebert, R. Kleppinger, J. H. Wendorff, *Liq. Cryst.* **1989**, *5*, 1841.

[35] G. Ungar, *Polymer* **1993**, *34*, 2050.

[36] R. Zhao, X. Jiang, J. Zheng, X. Liu, Y. Xu, S. Yang, E.-Q. Chen, *Acta Polym. Sin.* **2018**, *0*, 973.

[37] R. Zhao, T. Zhao, X. Jiang, X. Liu, D. Shi, C. Liu, S. Yang, E.-Q. Chen, *Adv. Mater.* **2017**, *29*, 1605908.

[38] X.-Q. Jiang, R.-Y. Zhao, W.-Y. Chang, D.-X. Yin, Y.-C. Guo, W. Wang, D.-H. Liang, S. Yang, A.-C. Shi, E.-Q. Chen, *Macromolecules* **2019**, *52*, 5033.

[39] G. Ungar, V. Percec, M. N. Holerca, G. Johansson, J. A. Heck, *Chemistry* **2000**, *6*, 1258.

[40] M.-H. Yen, J. Chaiprapa, X. Zeng, Y. Liu, L. Cseh, G. H. Mehl, G. Ungar, *J. Am. Chem. Soc.* **2016**, *138*, 5757.

[41] R. K. Josephson, *Annu. Rev. Physiol.* **1993**, *55*, 527.

[42] S. M. Mirvakili, I. W. Hunter, *Adv. Mater.* **2018**, *30*, 1704407.

[43] J. Luo, Z. Xie, J. W. Y. Lam, L. Cheng, B. Z. Tang, H. Chen, C. Qiu, H. S. Kwok, X. Zhan, Y. Liu, D. Zhu, *Chem. Commun.* **2001**, 1740.

[44] B.-K. An, S.-K. Kwon, S.-D. Jung, S. Y. Park, *J. Am. Chem. Soc.* **2002**, *124*, 14410.

[45] J. Shi, L. E. A. Suarez, S.-J. Yoon, S. Varghese, C. Serpa, S. Y. Park, L. Lüer, D. Roca-Sanjuán, B. Milián-Medina, J. Gierschner, *J. Phys. Chem. C* **2017**, *121*, 23166.

[46] J. Gierschner, S. Y. Park, *J. Mater. Chem. C* **2013**, *1*, 5818.

[47] J. Liao, M. Yang, Z. Liu, H. Zhang, *J. Mater. Chem. A* **2019**, *7*, 2002.

[48] R. Kaneko, Y. Sagara, S. Katao, N. Tamaoki, C. Weder, H. Nakano, *Chem.- Eur. J.* **2019**, *25*, 6162.

[49] J. Li, Z. Zhang, J. Tian, G. Li, J. Wei, J. Guo, *Adv. Opt. Mater.* **2017**, *5*, 1700014.

[50] J. Li, H. K. Bisoyi, J. Tian, J. Guo, Q. Li, *Adv. Mater.* **2019**, *31*, 1807751.

[51] S. Lin, K. G. Gutierrez-Cuevas, X. Zhang, J. Guo, Q. Li, *Adv. Funct. Mater.* **2020**, *31*, 2007957.

[52] P. Wei, J.-X. Zhang, Z. Zhao, Y. Chen, X. He, M. Chen, J. Gong, H. H.-Y. Sung, I. D. Williams, J. W. Y. Lam, B. Z. Tang, *J. Am. Chem. Soc.* **2018**, *140*, 1966.

[53] Y. Wu, S. Zhang, J. Pei, X.-F. Chen, *J. Mater. Chem. C* **2020**, *8*, 6461.

[54] D. Liu, D. J. Broer, *Liq. Cryst. Rev.* **2013**, *1*, 20.

[55] G. J. Fang, J. E. Maclennan, Y. Yi, M. A. Glaser, M. Farrow, E. Korblova, D. M. Walba, T. E. Furtak, N. A. Clark, *Nat. Commun.* **2013**, *4*, 1521.

[56] J. Vapaavuori, A. Laventure, C. G. Bazuin, O. Lebel, C. Pellerin, *J. Am. Chem. Soc.* **2015**, *137*, 13510.

[57] T. Yoshino, M. Kondo, J. Mamiya, M. Kinoshita, Y. Yu, T. Ikeda, *Adv. Mater.* **2009**, *22*, 1361.

[58] M. Kondo, Y. Yu, T. Ikeda, *Angew. Chem., Int. Ed.* **2006**, *45*, 1378.